The International Journal of Advanced Manufacturing Technology (2022) 123:357–372
https://doi.org/10.1007/s00170-022-10173-8

ORIGINAL ARTICLE

Analysis of drilling-induced geometrical damages in basalt and carbon fibre-reinforced polymer (BFRP and CFRP) composites

Gergely Magyar[1] · Dóra Károly[2] · Jinyang Xu[3] · Norbert Geier[1]

Received: 31 May 2022 / Accepted: 16 September 2022 / Published online: 28 September 2022

Abstract
Basalt fibre-reinforced polymer (BFRP) composites probably tend to replace some carbon fibre-reinforced polymer (CFRP) applications due to their excellent specific strengths and sustainability. Despite the published early promising results concerning the material properties of BFRP, their application is not widespread, and their machinability is not supported widely by published experiences. The main aim of the present study is to experimentally investigate the drilling-induced geometrical damages of BFRP and CFRP composites. Drilling experiments were conducted at various feed and cutting speed levels using a solid carbide twist drill. The drilling-induced burr was analysed by a Mitutoyo 361–804 digital microscope, a Mitutoyo SJ400 surface tester recorded the surface roughness, and the microstructure was analysed by a Zeiss Evo MA 10 scanning electron microscope. The measured data were evaluated through digital image processing (DIP), response surface methodology (RSM), and analysis of variances (ANOVA). The experimental results show that drilling-induced burr is more severe and surface roughness is worse in BFRP than in CFRP. The composite type influenced the geometrical damages primarily, followed by the feed in the case of burrs and by the cutting speed in the case of surface roughness. The present experimental study suggests that the drilling of BFRP is even more challenging than drilling CFRP from the point of view of burr formation and micro geometrical properties.

Keywords BFRP · CFRP · Drilling · Burr · Surface roughness · SEM

1 Introduction

Fibre-reinforced polymer (FRP) composites are popular in the high-tech sectors, mainly due to their excellent specific mechanical properties and corrosion resistance [1–3]. Despite the high-strength carbon fibres being the most applied reinforcing structures, the existing difficulties in manufacturing, reusing, or recycling carbon fibres encourage the application of more sustainable reinforcing materials; therefore, researchers investigate recently novel solutions like basalt fibres [4–6]. Although the material scientists are working on the material characterisation of basalt fibre-reinforced polymer (BFRP) composites and the results are promising [5–7], their application is still not widespread, and the existing experiences in their machining behaviour are severely deficient.

Amuthakkannan et al. [8] carried out drilling experiments to analyse the drilling-induced delamination of BFRP composites. They analysed the effect of cutting speed, feed rate, and point angle, each on three levels. Their results show that the cutting speed has the most significant influence on the delamination factor; nevertheless, the effect of the cutting speed was not considerable. Navarro et al. [9] performed edge trimming experiments with an uncoated carbide cutting inserts tool in BFRP composites to investigate the tool wear. They found that the cutting speed is the most crucial variable during edge trimming, which seems to be a contradictory finding relative to Amuthakkannan's, as the tool wear resulted in a

✉ Norbert Geier
geier.norbert@gpk.bme.hu

[1] Department of Manufacturing Science and Engineering, Faculty of Mechanical Engineering, Budapest University of Technology and Economics, Műegyetem rkp. 3., Budapest 1111, Hungary

[2] Department of Materials Science and Engineering, Faculty of Mechanical Engineering, Budapest University of Technology and Economics, Műegyetem rkp. 3., Budapest 1111, Hungary

[3] State Key Laboratory of Mechanical System and Vibration, School of Mechanical Engineering, Shanghai Jiao Tong University, Shanghai 200240, People's Republic of China

larger cutting edge radius has a significant impact on the cutting force and thus on the delamination. Navarro-Mas et al. [10] investigated the edge trimming-induced geometrical defect formation (delamination type I, II, and III) of BFRP composites. Their results show that the larger the cutting speed and feed rate, the larger the value of all three types of delamination in BFRP composites is. Navarro-Mas et al. [11] compared different parameters to evaluate delamination in BFRP composites. They found that–despite the delamination has a quasi-random nature–the delamination formation probability is lower at lower feed rates. The main reason is that lower feed rates result in smaller chip cross-sections and thus lower cutting force that is responsible for layer deconstruction of composites. The number of available studies on BFRP composite machining is limited, and their information on the machinability of BFRP is deficient. Therefore, the design and optimisation of machining processes of BFRP and thus the spread of these sustainable composites is not supported properly.

Even though the machinability of BFRP composites is not studied widely yet, their machining behaviour may be expected based on the extensive expertise in the machining of carbon fibre-reinforced polymer (CFRP) composites [12]. With the similarity in the material properties of the applied matrix materials (that are often epoxy resins) and the thin-fibrous high-strength reinforcing structures, the dominant chip removal mechanisms of BFRP composites are expected to be similar to the CFRP. Li et al. [13] orthogonally machined CFRP and observed that the chip removal mechanisms and chip morphology depend significantly on the fibre orientation and the depth of cut. They showed that the machined surface quality is significantly worst at larger fibre cutting angles. Wang et al. [14] highlighted that the cutting edge radius is also a significant parameter affecting the cutting mechanisms and surface generation. Hintze et al. [15] conducted drilling experiments in CFRP and confirmed that fibre orientation has a significant impact on the cutting mechanism. Furthermore, they concluded that the cutting force is a good response value to monitor, as it correlates to the sizes and amounts of machining-induced geometrical defects (e.g. delamination and burrs) around the hole. The fibre-orientation-based failure mechanisms of CFRP were investigated by Calzada et al. [16]. They highlighted that the fibre fracture is crushing-dominated between fibre cutting angles of 45° and 90° and is bending-dominated between 0° and 135°. Turki et al. [17] proved that each area around the drilled hole corresponds to the observations gained through orthogonal cutting experiments. In summary, the bending-dominated fibre fracture at unfavourable fibre cutting conditions ($\theta = 135° \pm \delta°$, where δ denotes error) around the machined hole significantly increases the risk of machining-induced geometrical error formation like delamination, burrs, fibre-pull-outs, and tearings [18].

Although the drilling-induced burrs do not weaken the resultant strength of the composite, burrs may become a potential starting point for further damage formations (e.g. delamination) and often result in assembly difficulties [19, 20]. Composite burrs are often measured and processed through digital image processing of optically captured images [21]. Xu et al. [22] observed that CFRP burrs in unidirectional fibrous laminates located symmetrically around the contour of the hole, depending significantly on the fibre cutting angle. Xu et al. [23] studied drilling-induced burrs in CFRP and found that the tool geometry has the most significant influence on the burr factor, followed by the cutting speed and feed rate, respectively. In contrast, some researchers found no relevant correlation between the feed and the burr characteristics [24–26]. Geier et al. [27] highlighted that drilling-induced burr formation in chopped CFRP is significantly influenced by fibre cutting angle and the mechanical supporting properties of the laminate.

Although the range of sustainable BFRP applications is getting more comprehensive, the experience and general understanding of the machining of basalt fibrous composites are lacking; therefore, the present study focuses on the experimental investigation of BFRP composites. The main objective of the present study is to analyse the machinability of BFRP composites through mechanical drilling experiments, focused on the analysis of drilling-induced burrs, surface roughness, and microstructure. The experimental results are compared to the observations of drilling CFRP composites. This study is structured as follows: first, the experimental setup and applied methods are presented in Sect. 2. Then, the results concerning burrs, surface roughness, and microstructure are presented in Sects. 3.1 and 3.2. Finally, optimal machining conditions are presented; and the results, limitations, and future aspects are discussed in Sect. 3.3.

2 Experimental setup and methods

2.1 Materials, tools, and machines

Two different composites were drilled in the experiments, provided by an industrial partner of the authors. One of them was a carbon fibre reinforcement polymer (CFRP) composite plate with a unidirectional (UD) reinforcement structure, vinyl-ester matrix, and nominal thickness of 5 mm. The second composite is a basalt fibre reinforcement polymer (BFRP) composite plate with a biaxial structure, epoxy resin, and nominal thickness of 10 mm. The main material characteristics–from the point of view chip removal mechanism–were measured five times, then averaged and

Table 1 Material properties of the applied CFRP and BFRP composites

Properties	BFRP	CFRP
Interlaminar shear strength (MPa)	18.85 ± 0.38	21.77 ± 0.70
Shore D hardness	82.78 ± 1.68	88.20 ± 0.40
Tensile strength (MPa)	465.04 ± 37.71	547.85 ± 45.78
Charpy impact strength (kJ/m^2)	162.18 ± 21.98	263.17 ± 24.76
Reinforcement type	Long basalt fibres	Long carbon fibres
Reinforcement structure	Bidirectional	Unidirectional
Matrix material	Epoxy resin	Vinyl-ester
Nominal sheet thickness (mm)	10	5

listed in Table 1. The tensile strength, interlaminar shear, shore D hardness, and Charpy impact strength were measured by a Zwick Z250 universal tensile tester (according to the ISO 527–5:1997 standard), Zwick Z005 universal tensile tester (MSZ EN ISO 14130:1998), Zwick H04.3150 hardness tester (MSZ EN ISO 868:2003), and Ceast Resil Impact Junior impact tester with a 15 J hammer (MSZ EN ISO 179–1:2010), respectively. Considering that the two composites differ not only by the fibre material, but in the reinforcement structure and matrix material also, the results have to be critically handled; i.e. the findings and observations cannot be explained by the change of a single "fibre material" factor but a material category factor having two levels: CFRP and BFRP.

The drilling experiments were carried out on a Kondia B640 three-axis CNC machining centre. A high-performance Nilfisk GB733 industrial vacuum cleaner was used during the experiments to remove the chips from the cutting space.

Table 2 Factors and their levels

Factor	Levels		
	−1	0	1
Material type		BFRP	CFRP
Cutting speed (m/min)	50	100	150
Feed (mm/rev)	0.05	0.10	0.15

A Tivoly Polaris 150 Sim Dim 6537K (82415011000) Ø10 mm diameter twist drill with titanium aluminium-nitride coating was used, as shown in Fig. 1b. The tool geometry is based on the DIN 6537k standard. The tool has a tip angle of 145°, helix angle of 35°, and transverse cutting edge length of 1 mm. A special fixture was used to fix the CFRP and BFRP composite plates. Therefore, the holes were drilled under the same mechanical support conditions. The tool condition was monitored during experiments using a Dino-Lite AM413ZT digital microscope. We did not observe the increase of the cutting edge radius; thus, the tool wear status did not change during the experiments. Images of the holes were taken with a Mitutoyo Quick Image QI-A505 optical microscope to examine the burr around the holes. The surface roughness of the holes was measured using a Mitutoyo SJ-400 contact surface tester. The surface integrity of the holes was investigated through a Zeiss Evo MA 10 scanning electron microscope (SEM). The experimental machining setup can be seen in Fig. 1a.

The experiments were designed with the central composite face-centred (CCF) design of experiment methods. The experimental design has three different factors: the material type as a categorical factor with two levels (BFRP and CFRP), and the cutting speed (v_c) and feed (f) as continuous factors with three levels each, as shown in Table 2.

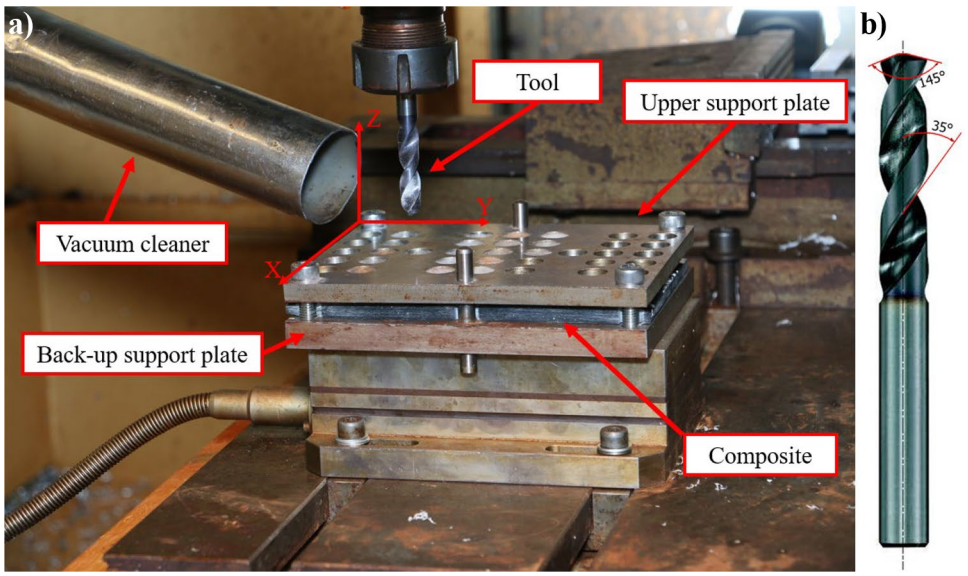

Fig. 1 The experimental machining setup: **a** working environment and **b** the applied coated solid carbide twist drill

The factor spaces and levels were determined based on suggestions of cutting tool producers and on previous studies [27, 28]. The drilling experiments were conducted in a dry condition, randomised order. The experimental setup in level zero ($v_c = 100$ m/min, $f = 0.10$ mm/rev) was repeated five times to calculate reproducibility and analysis of variances (ANOVA).

2.2 Methods

After the drilling experiments, images of the holes were taken with the Mitutoyo microscope and were evaluated using the following main steps (Fig. 2): First, the original image of the hole is uploaded to a Wolfram Mathematica program, as shown in Fig. 2a, then the contour of the hole with the burr is detected using edge detection (Fig. 2b), and its length is calculated. Then, the area of the burr is detected by comparing the previously detected contour and the nominal diameter of the hole, as can be seen in Fig. 2c. Finally, the burr area is calculated. The burr factor (F_b) and the contour burr factor (F_{bc}) were calculated according to Eqs. (1) and (2) [19].

$$F_b = \frac{A_{nom} - A_{free}}{A_{nom}} \cdot 100\% = \frac{A_b}{A_{nom}} \cdot 100\% \tag{1}$$

$$F_{bc} = \frac{C_b - C_{nom}}{C_{nom}} \cdot 100\% \tag{2}$$

where A_b (mm^2) is the burr area, A_{nom} (mm^2) represents the nominal area of the hole, and A_{free} denotes the burr-free area of the hole; C_b (mm) is the length of the contour of the machined geometry, and C_{nom} (mm) is the length of the ideal geometry.

The surface roughness was measured according to the ISO 4287:1997 standard, but the evaluation length was decreased to $L_e = 4$ mm because the length of the hole (5 mm in CFRP) was shorter than the standard. Each hole was measured five times in similar positions on the length of 2.5 mm. The speed of the detector was 1 mm/s, and the cut-off wavelength was set to 2.5 mm.

The micro-geometric properties of a machined surface carry several relevant information, such as the formation of fracture surfaces, the destruction mechanisms of fibres, or fibre matrix debonding [29]. A Zeiss Evo MA 10 scanning electron microscope was used for the investigation of these. Since the matrix materials of the workpieces are electrically insulating polymers, it was necessary to cover the surface with a conductive (golden) film with a BAL-TEC SCD 005 sputter coater machine (30-s cycles, with a current of 45 mA). The SEM images were taken with a 15 kV electron high tension (EHT) voltage. Several pictures were taken with different magnifications from the entry side (from which the tool penetrated the material), the middle section, and the exit side of the machined surface. Based on the images with good depth of field, the nature of the formed surfaces, the cutting and failure mechanisms, and the production quality of the workpieces were also established.

The quantitative results were evaluated using response graphs, which demonstrate the influences of factors on the corresponding responses. Response surface methodology (RSM) was used to develop these response surfaces. According to previous investigations [30], the effects of the process parameters on the analysed machining parameters are expected to be non-linear; therefore, a second-degree polynomial model was used to model, as shown in Eq. (3).

$$Y(x_1, x_2 \ldots x_n) = b_0 + \sum_{i=1}^{n} b_i x_i + \sum_{i=1}^{n} b_{ii} x_{ii}^2 + \sum_{i=1}^{n-1} \sum_{j=i+1}^{n} b_{ij} x_i x_j + \delta \tag{3}$$

where Y is the corresponding response value; x_i are the factors, b_0, b_i, b_{ij}, and b_{ii} are the regression coefficients of the parameters; and δ is a random experimental error. The analysis of variance (ANOVA) technique was used to analyse the significance level of the factor effects on the measured and calculated response values. The effect of a factor was considered significant if the ANOVA result has shown at least a significance level of $\alpha = 0.05$. The prediction accuracy of the RSM models was characterised by the percentage error (*PE*) parameter, as expressed by Eq. (4).

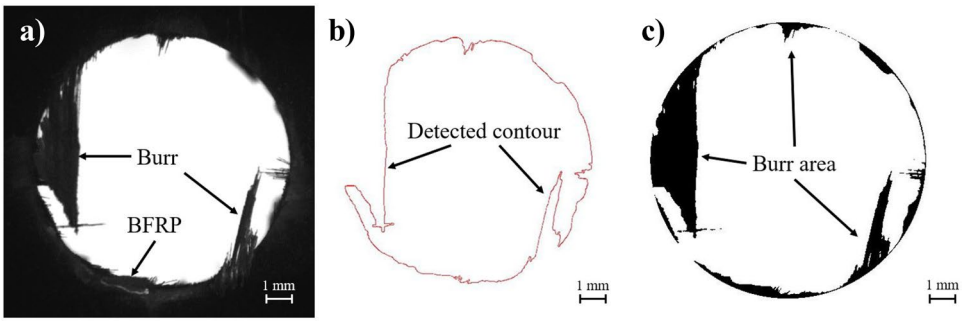

Fig. 2 Workflow of digital image processing of drilling-induced burrs in fibrous composites: **a** original image, **b** detected contour of the burr (C_b), and **c** burr area (A_b)

$$PE_i = \left| \frac{Y_i - Y_m}{Y_m} \right| \cdot 100\% \quad (4)$$

3 Results and discussion

In this section, the experimental results concerning burrs, surface roughness, and microgeometry are presented, optimised, and discussed. The measured, calculated, and predicted response parameters (burr factor, contour burr factor, arithmetical mean height, and maximum height of profile) are summarised in the appendix (Table 5).

3.1 Analysis of drilling-induced burrs

The calculated burr factor (F_b) and contour burr factor (F_{bc}) values are summarised in the Appendix (Table 5) and illustrated in Fig. 3. The processed images suggest that the drilling-induced burrs were more severe in the BFRP than in the CFRP composite. This is in good agreement with the observations of Fu et al. [31], as they pointed out that the drilling-induced damage formation in MD composites is more severe than in UD composites. In the case of drilling MD composite, one cutting edge gets contact four times with the technologically disadvantageous fibre cutting angles ($\theta = 135° \pm \delta°$), while this contact number is only two in the case of unidirectional composites. Therefore, the more the fibre reinforcement direction, the larger the probability of machining-induced defect formation is. Nevertheless, a non-expected difference in the influence of process parameters on the burr parameters was found, as shown in Fig. 4 and discussed below.

The RSM-based mathematical models predicting the burr factor and the contour burr factor in the case of BFRP and CFRP are expressed by Eqs. (5)–(8). The visualisations of these mathematical models in 3D response diagrams are shown in Fig. 4. These response diagrams illustrate the effect of the process parameters on the burr factor and the contour burr factor. The average percentage errors for the RSM models predicting F_b and F_{bc} in BFRP are 36.42%, 20.80%, and in CFRP 28.95% and 16.89%, respectively.

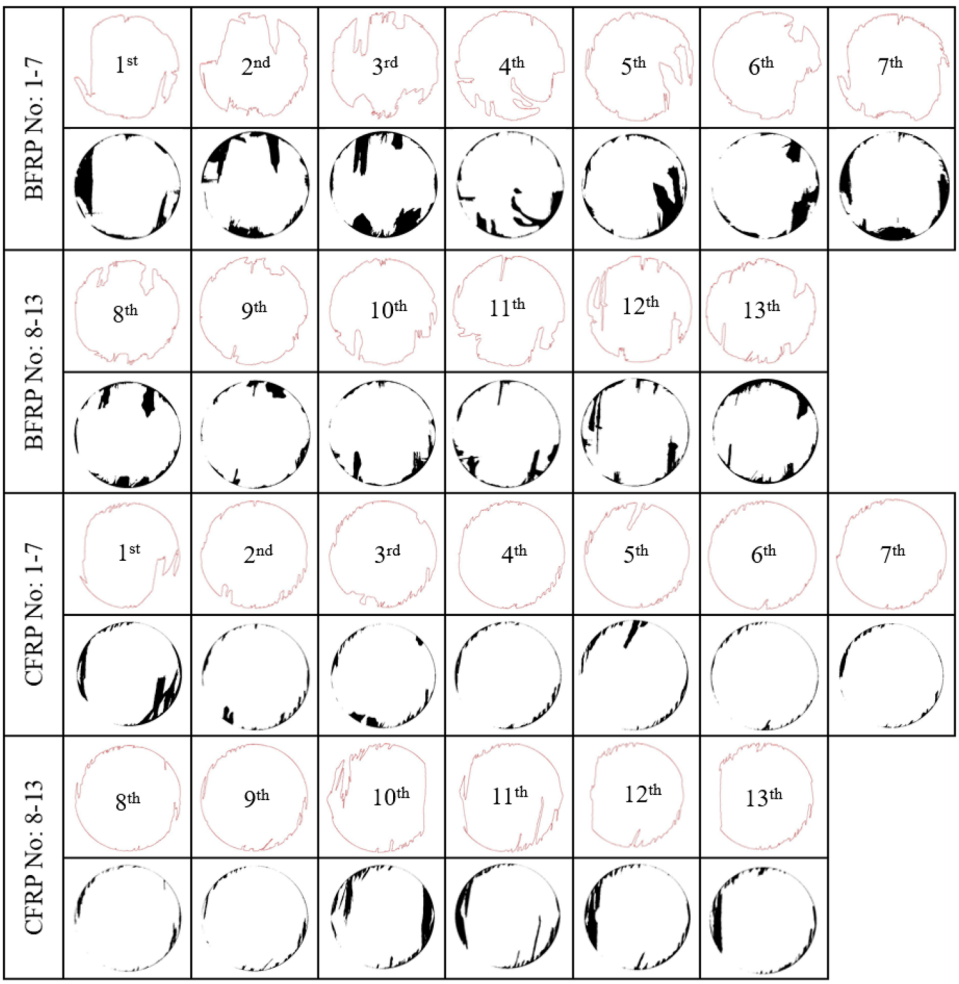

Fig. 3 Processed images of drilled hole exit in BFRP and CFRP composites

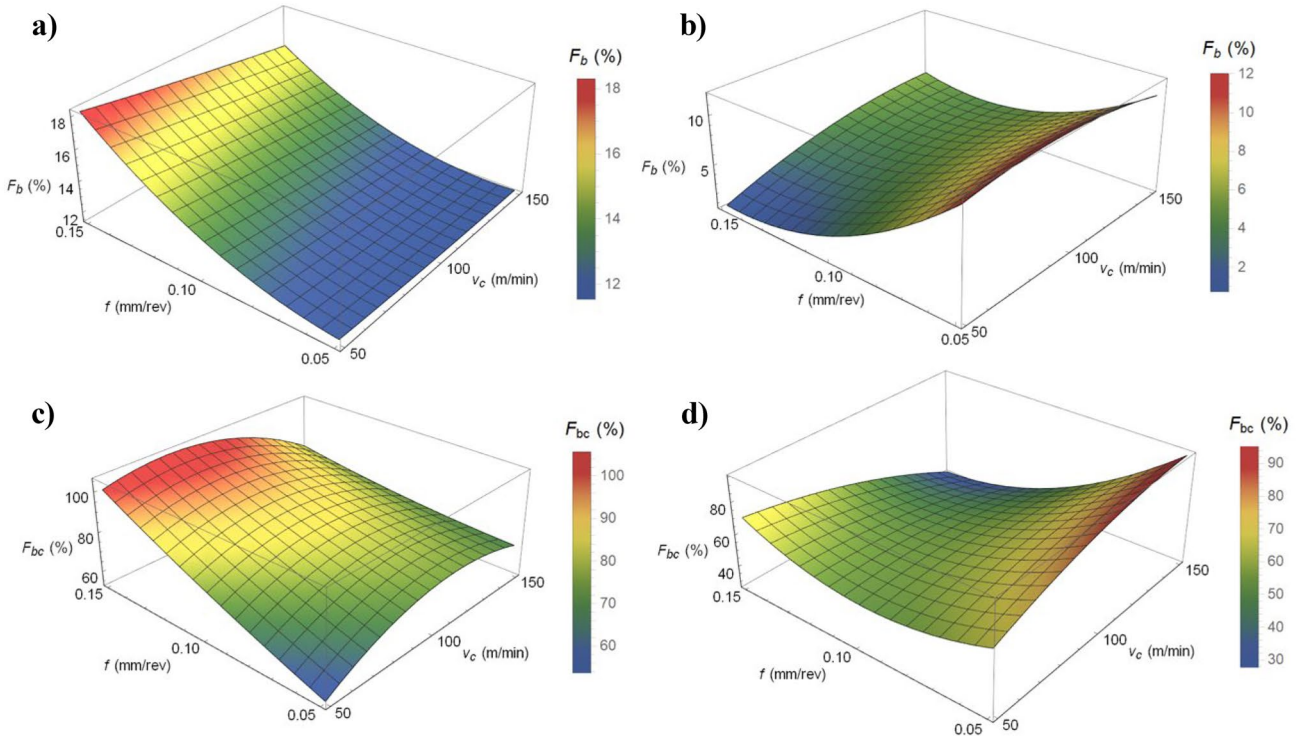

Fig. 4 The effect of process parameters on the burr factor and the contour burr factor after drilling **a**, **c** BFRP and **b**, **d** CFRP composites

These drilling-induced burr prediction accuracies are not as prominent as they are influenced primarily by the tool condition, as pointed out by Hrechuk et al. [21].

$$F_b^{BFRP} = 12.2 - 30f + 0.003v_c + 536f \cdot f + 0.000034v_c \cdot v_c - 0.224f \cdot v_c \quad (5)$$

$$F_b^{CFRP} = 23.72 - 376f + 0.060v_c + 1233f \cdot f - 0.000456v_c \cdot v_c + 0.516f \cdot v_c \quad (6)$$

$$F_{bc}^{BFRP} = -19 + 501f + 1.35v_c + 765f \cdot f - 0.00511v_c \cdot v_c - 3.58f \cdot v_c \quad (7)$$

$$F_{bc}^{CFRP} = 61.4 - 886f + 1.13v_c + 6487f \cdot f - 0.00237v_c \cdot v_c - 7.24f \cdot v_c \quad (8)$$

ANOVA results (Table 3) and the main and cross-effect plots (Fig. 5) show that the type of the composite (whether it is BFRP or CFRP) significantly influences the F_b and F_{bc} parameters (F-value = 20.54, P-value = 0.000 for F_b, and F-value = 7.08, P-value = 0.016 for F_{bc}). Despite the P-values of the feed (0.566 and 0.903) in the ANOVA table suggesting that the effect of the feed is not significant, its interaction with the composite type is significant. This means that the effect of feed is significantly influenced by whether the CFRP or the BFRP is drilled. The larger the feed, the larger the probability of burr formation in the BFRP is. However, the opposite was observed in the CFRP. This reason may be that the larger the feed, the larger the chip thickness is; therefore, larger energy is needed to bend the last laminated CFRP layers. In the literature, there is still disagreement whether the larger feed results in larger burrs in fibrous composites or not, as the mechanical supporting circumstances and the tool condition play a more critical role in burrs formation [19].

Generally, more drilling-induced burrs were formed in the BFRP, possibly due to the more-difficult cutting nature and multidirectional reinforcement structure than the CFRP. The BFRP and CFRP composites seem to be similarly destroyed (the contour of the burrs have similar lengths), as the similar F_{bc} parameters and images in Fig. 3 prove. The ANOVA resulted that the cutting speed has no relevant influence on the drilling-induced burr formation neither in the BFRP nor the CFRP.

3.2 Analysis of surface integrity

Although the machined surface characteristics are often not the critical parameters to be optimised during the drilling of fibre-reinforced composite materials, it is a general characterisation of the machinability of a material [32–35]. In this section, we report the results obtained from investigating the integrity of the drilled surfaces by examining the effects associated with the measured surface roughness values and analysing the formed surfaces through scanning electron microscopy.

Table 3 ANOVA table for the burr factor and contour burr factor

Source	Burr factor (F_b)					Contour burr factor (F_{bc})				
	DF	Adj SS	Adj MS	*F*-value	*P*-value	DF	Adj SS	Adj MS	*F*-value	*P*-value
Model	8	358.184	44.773	4.93	0.003	8	7022.2	877.77	1.98	0.113
Linear	3	188.960	62.987	6.94	0.003	3	3154.4	1051.46	2.37	0.107
f	1	3.117	3.117	0.34	0.566	1	6.7	6.74	0.02	0.903
v_c	1	0.217	0.217	0.02	0.879	1	33.7	33.70	0.08	0.786
Composite	1	186.520	186.520	20.54	**0.000**	1	3140.3	3140.27	7.08	**0.016**
Square	2	23.174	11.587	1.28	0.305	2	643.5	321.75	0.73	0.499
f·f	1	22.943	22.943	2.53	0.130	1	495.0	495.03	1.12	0.306
v_c·v_c	1	1.959	1.959	0.22	0.648	1	392.4	392.40	0.88	0.360
2-way interaction	3	137.533	45.844	5.05	0.011	3	3776.7	1258.90	2.84	0.069
f·v_c	1	0.171	0.171	0.02	0.893	1	1380.8	1380.77	3.11	0.096
f·*composite*	1	112.686	112.686	12.41	**0.003**	1	2507.1	2507.08	5.65	**0.029**
v_c·*composite*	1	6.296	6.296	0.69	0.417	1	3.1	3.05	0.01	0.935
Error	17	154.388	9.082			17	7542.5	443.68		
Lack-of-fit	7	104.651	14.950	3.01	0.056	7	2407.1	343.87	0.67	0.695
Pure error	10	49.737	4.974			10	5135.4	513.54		
Total	25	512.572				25	14,564.7			

Bold entries denote *P*-values lower than 0.05, indicating that the particular factor has a significant effect

3.2.1 Surface roughness

The results of the surface roughness measurement, such as arithmetical mean height (R_a) and maximum height of profile (R_z), are listed in the Appendix (Table 5). The surface roughness parameters were calculated based on the ISO 4287:1997 standard. The experimental results demonstrate that the measured surface roughness is much less favourable for the BFRP composite than for the CFRP composite. The reason for this may be found in the biaxial reinforcement structure of the BFRP, as there are far more uncut or crushed fibres (as discussed later in the SEM investigations) in the BFRP composite holes, thus resulting in rougher surface quality. The developed RSM models predicting the R_a and R_z values are expressed by Eqs. (9)–(12). The visualisations of these models representing the effect of the process parameters are shown in Fig. 6 in 3D response graphs. The average percentage errors for the RSM models predicting R_a and R_z in BFRP are 15.80% and 10.67%, and in CFRP are 13.69% and 17.40%, respectively. These prediction accuracies are better than the prediction accuracy of drilling-induced burr, as the selected factors (feed and speed) have theoretically a more vital role in surface generation than burr formation.

$$R_a^{BFRP} = 14.76 + 15f - 0.18v_c - 473f \cdot f + 0.000711v_c \cdot v_c + 0.928f \cdot v_c \quad (9)$$

$$R_a^{CFRP} = -3.31 + 99.9f + 0.0306v_c - 353f \cdot f + 0.000127v_c \cdot v_c - 0.223f \cdot v_c \quad (10)$$

$$R_z^{BFRP} = 70.0 + 258f - 0.687v_c - 3150f \cdot f + 0.00288v_c \cdot v_c + 3.80f \cdot v_c \quad (11)$$

$$R_z^{CFRP} = 25.5 - 252f + 0.177v_c + 1083f \cdot f - 0.00007v_c \cdot v_c + 0.32f \cdot v_c \quad (12)$$

In the case of both composites, the response graphs show a similar characteristic. This is in a good correlation with

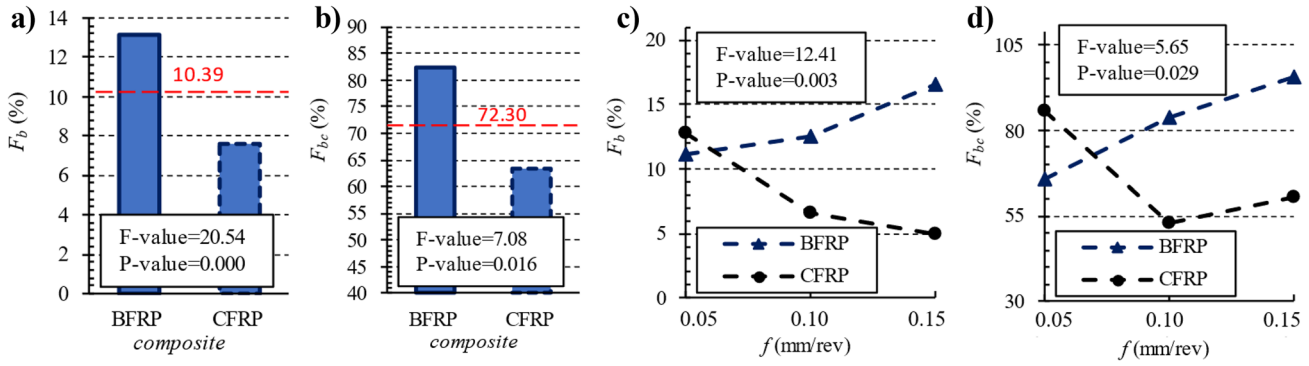

Fig. 5 Main effect plots of the type of the composite for **a** F_b and **b** F_{bc} and the interaction of feed vs composite on the **c** F_b and **d** F_{bc}

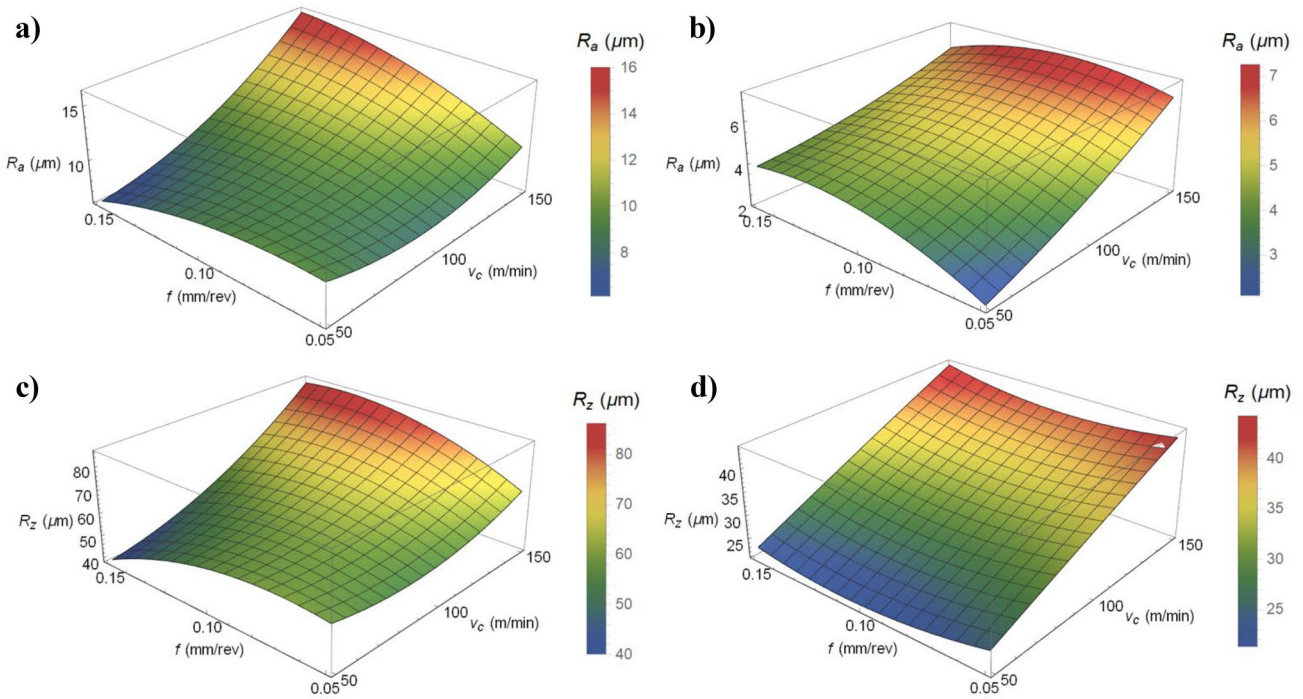

Fig. 6 The effect of process parameters on the arithmetical mean height of hole wall surface in **a** BFRP and **b** CFRP composites and on the maximum height of profile of hole wall in **c** BFRP and **d** CFRP composites

results of ANOVA (Table 4), which shows that the cutting speed (F-value = 21.93, P-value = 0.000 for R_a, and F-value = 22.78, P-value = 0.000 for R_z) and the type of the composite (F-value = 45.72, P-value = 0.000 for R_a, and F-value = 68.77, P-value = 0.000 for R_z) have significant effect on both surface roughness metrics. However, ANOVA results show that the feed does not significantly influence the surface roughness parameters. It seems contradictory to the machining theory, as the larger the feed, the larger the distance between roughness valleys; thus, the worse the surface quality is [36–38]. The possible reason for the neutral effect of the feed on surface roughness may be that the variation

Table 4 ANOVA table for arithmetical mean height and maximum height of profile

Source	Arithmetical mean height (R_a)					Maximum height of profile (R_z)				
	DF	Adj SS	Adj MS	F-value	P-value	DF	Adj SS	Adj MS	F-value	P-value
Model	8	259.137	32.392	9.63	0.000	8	7710.36	963.80	12.56	0.000
Linear	3	236.940	78.980	23.48	0.000	3	7278.33	2426.11	31.63	0.000
f	1	7.403	7.403	2.20	0.156	1	21.23	21.23	0.28	0.606
v_c	1	73.747	73.747	21.93	**0.000**	1	1747.24	1747.24	22.78	**0.000**
Composite	1	153.756	153.756	45.72	**0.000**	1	5274.86	5274.86	68.77	**0.000**
Square	2	11.587	5.794	1.72	0.208	2	122.48	61.24	0.80	0.466
f·f	1	4.335	4.335	1.29	0.272	1	28.77	28.77	0.38	0.548
v_c·v_c	1	10.803	10.803	3.21	0.091	1	120.98	120.98	1.58	0.226
2-way interaction	3	13.395	4.465	1.33	0.298	3	282.76	94.25	1.23	0.330
f·v_c	1	11.629	11.629	3.46	0.080	1	240.59	240.59	3.14	0.094
f·*composite*	1	0.389	0.389	0.12	0.738	1	11.66	11.66	0.15	0.701
v_c·*composite*	1	0.122	0.122	0.04	0.851	1	3.25	3.25	0.04	0.839
Error	17	57.176	3.363			17	1304.01	76.71		
Lack-of-fit	7	35.133	5.019	2.28	0.115	7	744.50	106.36	1.90	0.172
Pure error	10	22.043	2.204			10	559.51	55.95		
Total	25	316.312				25	9014.37			

Bold entries denote P-values lower than 0.05, indicating that the particular factor has a significant effect

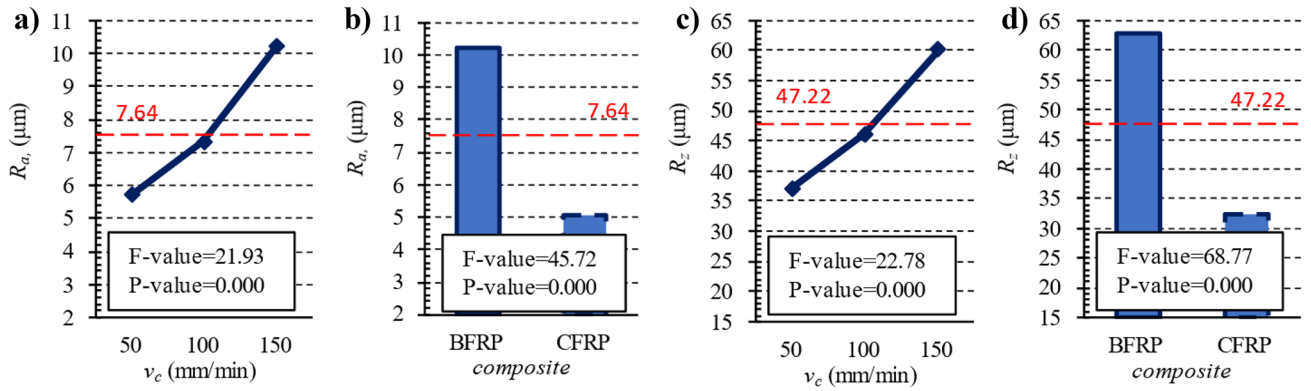

Fig. 7 Main effect plots of significant factors (v_c and *composite*): on the arithmetical mean height of **a** BFRP and **b** CFRP, and on the maximum height of profile of **c** BFRP and **d** CFRP composites

interval of the feed factor was small. A wider range of feeds would be beneficial to analyse in the future. ANOVA results prove that none of the interaction terms is significant on the surface roughness parameters.

The main effect plots of factors that significantly influence the responses are shown in Fig. 7. The larger the cutting speed, the worse the R_a and R_z parameters are in both composites. The higher speeds often result in higher cutting power and, therefore, in higher cutting temperatures; thus, there is a possibility that the matrix is more likely to plastically deform and smear instead of being cut [39]. Furthermore, the surface was rougher in the BFRP than in the CFRP. The machined surfaces are analysed through scanning electron microscopy and discussed in the next section to find the proper reason for this.

The ratio of R_z to R_a is a representative quality parameter showing whether the amount of uncut materials (fibre, matrix, non-reinforcing fibres, etc.) is remarkable compared to the average surface quality [32]. The scatterplot of R_z versus R_a for the BFRP and CFRP composites is shown in Fig. 8. The slopes of the fitted linear models to the measurements show that the R_z/R_a for the BFRP composite (5.86) is not significantly different from the CFRP's (5.10). This suggests that the specific amount of uncut fibres (bent instead of being cut at the nominal depth) on the machined surfaces of BFRP and CFRP composites significantly does not differ.

3.2.2 SEM investigations

The SEM images show all the essential properties (feed direction, value of the fibre cutting angle –θ, etc.) and characteristic elements (debris, cavities, fracture surfaces, etc.) separately. Figure 9 shows the entry side of the drilled composites. The machined surface of the CFRP material is less rough, but the surface properties change enormously

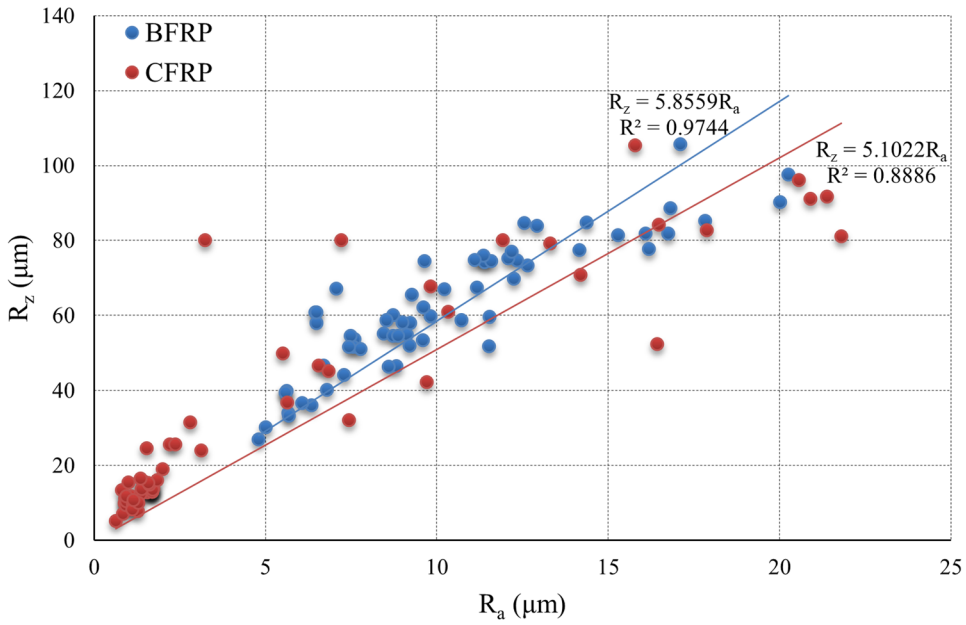

Fig. 8 Scatterplot of maximum height of profile versus arithmetical mean height in BFRP and CFRP composites

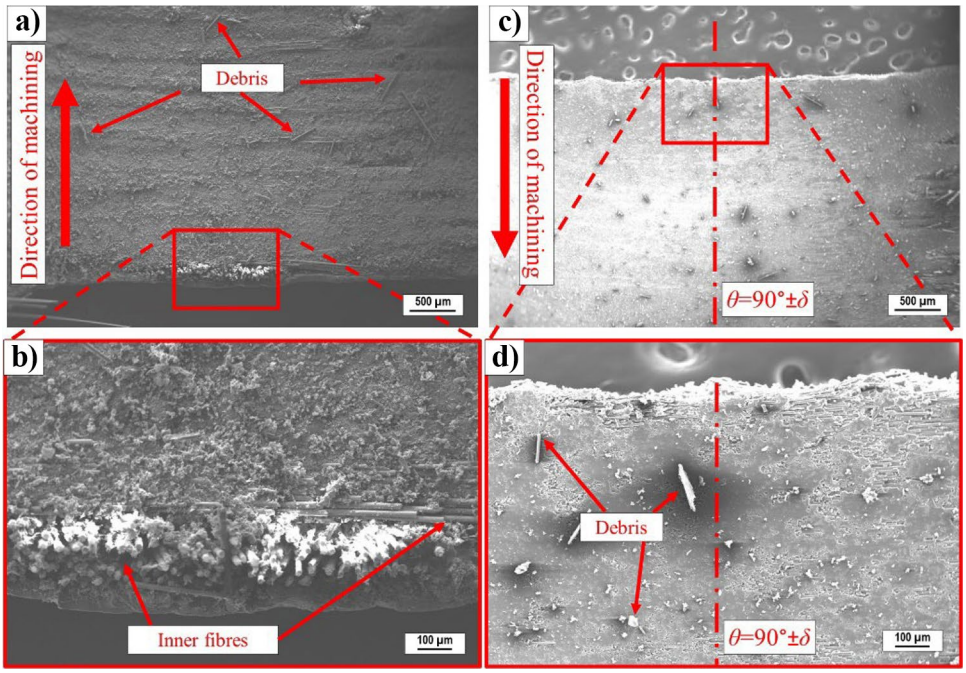

Fig. 9 SEM images on the entry side of drilled composite holes in **a**, **b** BFRP and **c**, **d** CFRP composites

with the change of the fibre cutting angle, while in the case of the BFRP composite, the surface is almost uniform but rougher. This means that the significant difference in the previously presented surface roughness between the BFRP and CFRP composites is not caused primarily by the different reinforcing structures (and thus the fibre cutting angle) but by the composite material characteristics (i.e. matrix rigidity, reinforcing fibre strength). The presence of debris can be observed on both composites. In the case of the BFRP composite, due to the structure of the fabric, the fibres at the edge of the workpiece point towards the inside of the hole resulting in uncut fibres, while in the case of the CFRP material, this phenomenon does not occur at the same fibre cutting angles. This partly explains why the BFRP material was more prone to higher burr formation. In the case of CFRP, although the interior structure of the surface is highly dependent on the direction of the fibres, there is no significant difference at the edge of the material.

Figure 10 shows the exit side of the holes. More significant material defects tend to occur on the exit side of the

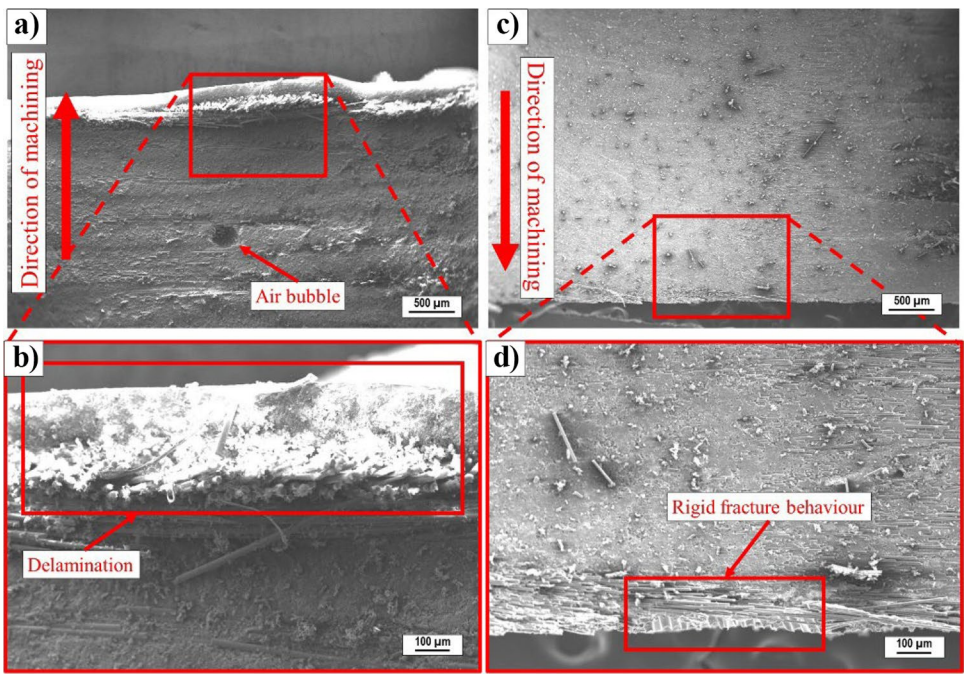

Fig. 10 SEM images on the exit side of drilled composite holes in **a**, **b** BFRP and **c**, **d** CFRP composites

hole after drilling fibre-reinforced composites [40], as was observed in this study also. An independent manufacturing defect in the form of an air bubble can be observed in Fig. 10a. The possible reason for this error is that during the manual lamination, it was not possible to remove all the air from the material, so during the curing of the matrix, it remained there, causing a material shortage. With mass production technology (like in the case of the CFRP material), such defects are less typical than in the case of manual lamination. However, Fig. 10b, d show typical exit side defects, delamination in the case of the BFRP material, and a brittle fracture surface of the matrix material in the case of the CFRP material. Delamination is a characteristic and severe defect of fibre-reinforced polymer composites [41]. The reason for delamination formation is that the connection between the layers of reinforcing material cannot provide sufficient rigidity for the tool to cut (i.e. the thrust force reaches the critical thrust force [42]), but the force in the feed direction pushes the material in front of it, the layers separate, and the separated layers remain in this shape on the resulting machined surface after cutting ceases. This phenomenon may also be related to the formation of burrs, and here, too, the fibres point towards the inside of the hole. In the case of CFRP, the brittle fracture surface results from the brittleness of the vinyl ester matrix material. There may have fewer reinforcing fibres and more matrix material around the fracture surface, so the feed force broke the remaining material instead of being able to cut it. The surface of the inner part of the hole depends on the fibre direction for CFRP, but less for BFRP. However, the properties of the immediate environment of the exit do not depend on the fibre direction. The inner part of the exit side is similar to the inner part of the entry side. The surface of the BFRP material is rougher, more debris and protruding fibres are observed than in the case of CFRP, and the surface quality of CFRP is highly dependent on the fibre cutting angle.

Figure 11 shows the middle section of the hole in both composites. In Fig. 11a1, a2, the layers of the biaxial reinforcement can be observed in the BFRP material. Although there is no significant effect of the direction of the fibres on the fabric structure, it can be observed that during cutting, the tool (i) cuts the reinforcing fibres, (ii) cuts off the matrix material from the fibres and makes the fibres bundles visible, and (iii) pulls out the fibres from the matrix and form voids on the surface in some part of the material. These parts do not cause a very different surface structure, the overall surface quality is similar, and this phenomenon does not cause any significant effect during the practical use of the material. In Fig. 11a3, a4, the adhesion between the elementary fibres and the matrix and the generally sheared surface on the elementary fibres can also be observed in the BFRP material. There is also an interesting phenomenon in which the tool did not sheared the fibres but penetrated them and did not cut the entire cross-section, but only twisted part of the fibres. This phenomenon can be explained by the relationship between cutting and fibre direction. However, it can still be said that in the case of BFRP with a biaxial reinforcement structure, this fibre direction has no significant effect on either the machinability or the practical applicability.

Figure 11b1–b4 shows the middle section of the CFRP material. As on the BFRP material, the adhesion between the elementary fibres and the matrix material can be observed here. In this case, the cutting angle significantly affects the surface formed after cutting. Going from left to right in the figures, there is a significant change in the quality of the machined surface due to the change in the fibre cutting angle. At a cutting angle of 90°, the reinforcing fibres are sheared and have no particular effect on the surface quality (Fig. 11b1). At a cutting angle of 110°, only the matrix material is removed, and the elementary fibres are shown. Typically, sheared surfaces can be observed here. Since the diameter of the carbon fibres is smaller than that of the basalt fibres, no twisted fibres were found during the surface examination. In Fig. 11b3–b4, at a cutting angle of 135°, the tool cuts the reinforcing fibres, then pushes them in front of them and pulls them out of the matrix material, creating a highly rough, uneven surface. When the tool starts to push the fibres in front of it, much greater forces occur than in other cases. Thus, with a strong exaggeration, it can also be considered a kind of interrupted cutting. Furthermore, this area also explains why the surface roughness is so different in different parts of the hole. For CFRP, the best surface quality is obtained for fibre cutting angles less than 90°. A very smooth, uniform surface can be observed in these areas (except debris) due to the smearing of the matrix material on the surface.

Comparing Fig. 11a2, b2, the degree of adhesion between the matrix material and the reinforcing fibres is very similar for the two composites. The difference between fibre production technologies was not a relevant factor in this respect.

3.3 Optimisation, discussion, and outlook

The optimal drilling conditions to minimise each analysed quantitative response parameter (F_b, F_{bc}, R_a, R_z) are calculated through multi-objective optimisation in the Minitab software, and it is characterised by a feed of 0.05 mm/rev and cutting speed of 72.2 m/min in the BFRP, and feed of 0.11 mm/rev and cutting speed of 50 m/min in the CFRP. The multi objective-optimisation is illustrated in Fig. 12. In the case both materials can

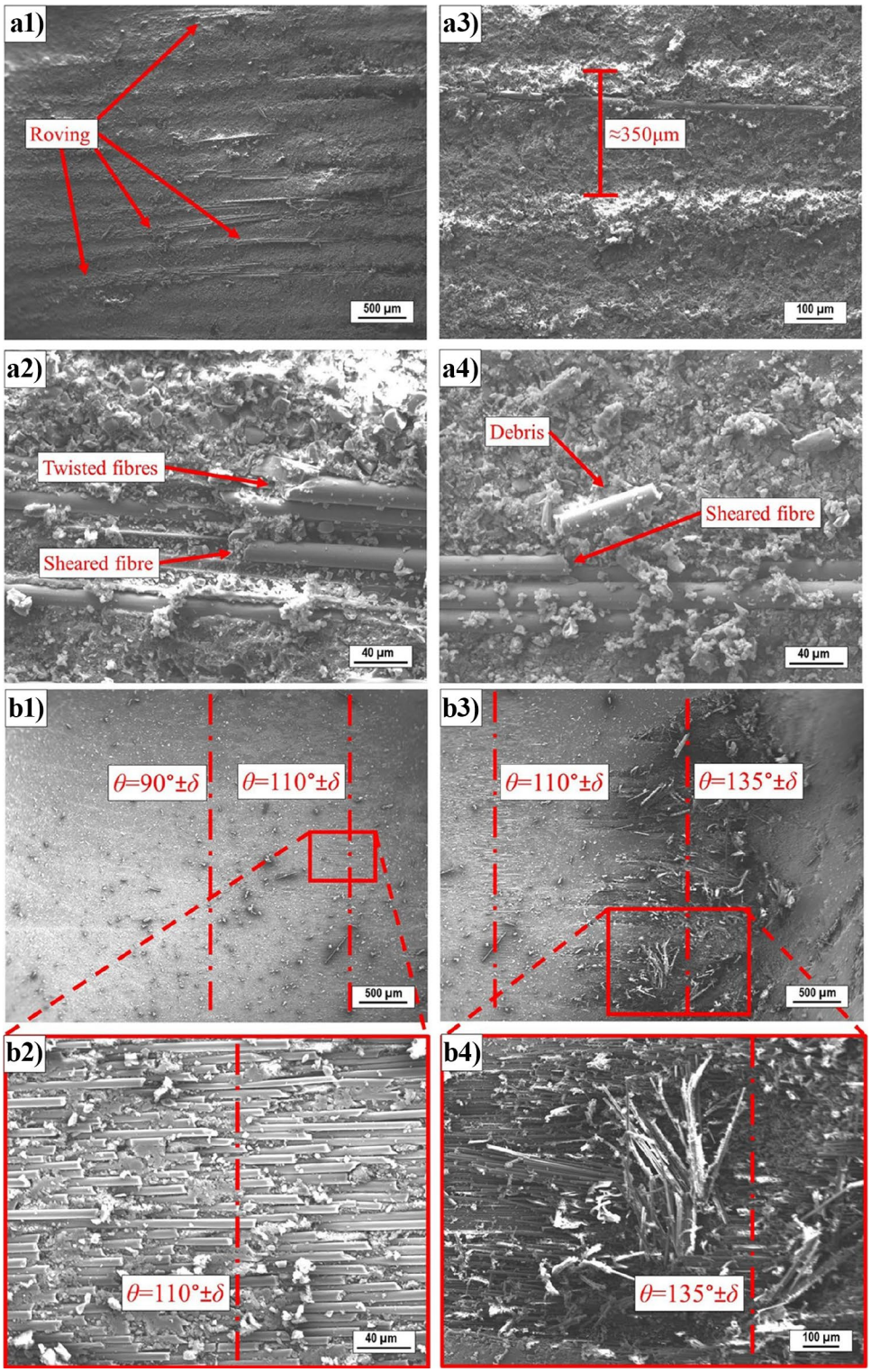

Fig. 11 SEM images on the middle section of drilled composite holes in **a1**–**a4** BFRP and **b1**–**b4** CFRP composites

meet the requirements of the designers (having appropriate strength, dimensional stability, etc.), the application of the CFRP is recommended from the point of view of minimising the machining-induced geometrical defect formation. Furthermore, if sustainability is one of the main critical criteria of composite material selection, the

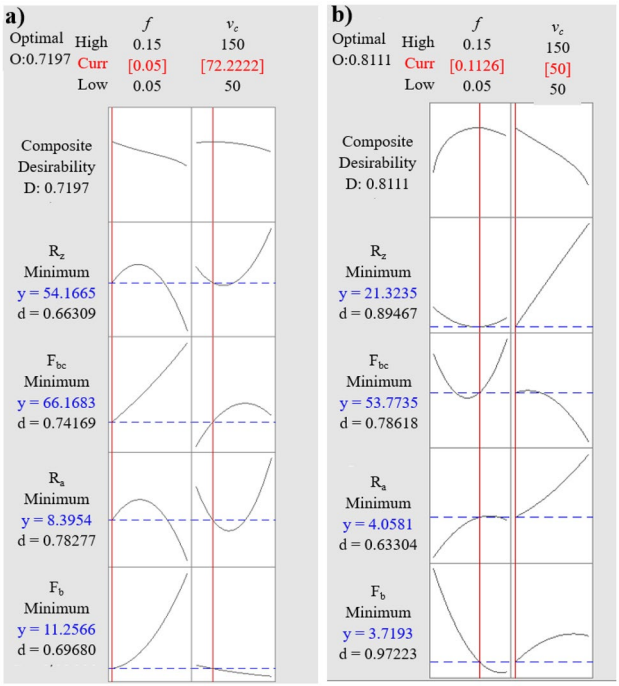

Fig. 12 Multi-objective optimisation of drilling in **a** BFRP and **b** CFRP composites to minimise F_b, F_{bc}, R_a, and R_z parameters

BFRP is possibly the right choice. The analysis of cutting energetics (cutting force, torque, and vibrations) is one of the next steps in this research project.

It is essential to highlight that the applied BFRP and CFRP composites cannot be compared correctly enough, as their optimal layering sequence, reinforcement structures, applied matrix materials, etc. differ in industrial applications. Thus, if these composites are compared from a certain point of view (burr formation, surface generation, etc.), these composites are better to consider as category factors (like A and B material). Otherwise, if only the reinforcement material (carbon and basalt) is varied systematically in the design of experiments, the obtained results would fail to present relevant information for the industrial applications. Nevertheless, the analysis of the influences of reinforcing fibres on the cutting mechanism is essential in the future to deeper understand the machinability of BFRP composites.

Although the present study suggests that the BFRP composite machining is even more challenging than the machining of CFRP, the interpretation of the findings and observations into industrial scales needs further and more detailed investigations on the chip removal mechanisms, and delamination and burr formation mechanisms of BFRP. Furthermore, as the tool condition has the most significant influence on the machining mechanisms, the tool wear mechanisms and speed of tool wear in the machining of BFRP are recommended to be analysed in the future.

4 Conclusions

In the present experimental study, the machinability of basalt fibre reinforced polymer (BFRP) was investigated by analysing drilling-induced burrs, surface roughness, and microstructure. The results were then compared with the observations gained in carbon fibre-reinforced polymer (CFRP) composite drilling. According to the present study, the following conclusions can be drawn:

- More severe drilling-induced burr formation was observed in the BFRP composite than in the CFRP. The composite-feed interaction influenced the burr formation in the composites. The larger the feed, the larger the drilling-induced burrs are in the BFRP. However, the opposite phenomenon was observed in the CFRP composite. The influence of the cutting speed was not considerable; thus, the feed is recommended to be optimised to minimise burrs.
- ANOVA results show that the composite type has the most significant influence on the surface roughness, followed by the cutting speed. However, the effect of the feed was not considerable in each composite. Both the arithmetical mean height and maximum height of profile of BFRP was worse than those of CFRP. The interaction terms were not significant.
- It was observed through SEM investigation that the main reasons for the differences between the BFRP and CFRP surfaces are the differences between the structure, the matrix material, and the diameter of the fibres. A less rough surface is obtained for CFRP, except for the region around the 135° cutting angle. In the case of the vinyl-ester matrix material, the smear of the material was characteristic, while in the case of the epoxy, this was not typical; much larger particles were observed. Respectively, in the case of CFRP, the shear surface was observed in the fibres, while in the case of

BFRP, the twisted elementary fibres were also visible due to the thicker fibres.

- The optimal conditions to drill suitable quality holes in BFRP are characterised by the feed of 0.05 mm/rev and cutting speed of 72.2 m/min, and feed of 0.11 mm/rev and cutting speed of 50 m/min in the CFRP. From the point of view of drilling-induced micro and macro geometrical damage formation, the CFRP is recommended to apply. However, the analysis of chip removal and tool wear mechanism in BFRPs is recommended in the future to obtain more significant regularities and a generous understanding of BFRP machining.

Appendix

Table 5 Experimental design table showing the measured, calculated and percentage error of RSM models

No.	Factors		BFRP								CFRP							
			Measured				Percentage error (*PE*)				Measured				Percentage error (*PE*)			
	f (mm/rev)	v_c (m/min)	F_b (%)	F_{bc} (%)	R_a (μm)	R_z (μm)	F_b (%)	F_{bc} (%)	R_a (%)	R_z (%)	F_b (%)	F_{bc} (%)	R_a (μm)	R_z (μm)	F_b (%)	F_{bc} (%)	R_a (%)	R_z (%)
1	0.05	50	15.26	60.75	7.31	47.89	4.74	11.54	28.87	16.49	13.58	60.24	2.16	26.02	4.54	9.21	3.21	3.62
2	0.15	100	16.69	87.44	8.07	52.83	25.37	18.44	16.40	11.48	5.02	55.07	5.90	44.91	7.51	0.16	20.04	24.59
3	0.15	50	20.60	112.08	5.75	35.64	11.34	9.68	6.20	24.71	6.33	66.87	3.41	20.87	84.06	5.78	14.61	10.88
4	0.10	100	11.75	98.23	10.80	59.02	33.98	11.58	8.12	3.07	4.64	45.08	5.02	30.33	38.49	21.04	4.590	3.31
5	0.10	100	16.37	99.68	8.85	58.83	3.84	12.87	12.12	3.40	6.17	72.45	5.30	37.78	4.28	24.68	1.02	17.08
6	0.10	100	12.41	42.47	12.33	71.22	26.80	104.51	19.52	14.58	5.20	40.06	5.88	34.69	23.73	36.23	10.72	9.70
7	0.10	150	15.56	65.10	12.88	77.92	5.76	11.48	12.14	1.94	7.29	39.89	7.33	41.84	13.86	13.43	1.05	2.23
8	0.15	150	12.54	87.08	17.93	90.64	52.67	7.74	9.41	7.83	3.65	59.47	4.06	25.12	88.73	53.36	51.82	76.10
9	0.10	50	7.19	58.41	11.41	69.15	136.80	29.40	21.56	24.18	3.44	69.09	3.67	18.43	7.05	24.68	5.86	16.12
10	0.05	100	8.57	65.42	10.30	64.07	62.92	13.05	21.57	9.26	13.38	104.82	7.01	45.87	14.41	17.55	42.69	25.43
11	0.05	150	9.44	71.54	10.22	64.92	44.01	4.06	0.68	8.88	11.19	91.92	6.07	38.90	20.72	3.56	8.32	10.49
12	0.10	100	10.62	134.33	6.73	54.28	48.12	35.34	47.43	12.07	10.72	49.99	4.75	30.13	40.03	9.17	10.41	4.00
13	0.10	100	13.44	87.46	10.06	60.79	17.06	0.70	1.41	0.06	9.05	54.94	5.45	25.55	28.96	0.68	3.61	22.63

Acknowledgements The authors acknowledge the support of Dániel István Poór, Csongor Pereszlai, Tamás Lukács, Zsolt Hodosán, and Péter Tamás-Bényei in the experimental work.

Author contribution Gergely Magyar: resources, investigation, formal analysis, visualisation, software, writing–original draft; Dóra Károly: investigation, validation, writing–original draft; Jinyang Xu: writing–review and editing, supervision; Norbert Geier: conceptualisation, methodology, writing–review and editing, supervision.

Funding Open access funding provided by Budapest University of Technology and Economics. This research was partly supported by the National Research, Development and Innovation Office (NKFIH) No. OTKA-PD20-134430 and ÚNKP-21–2-I-BME-237; and by the 9th Sino-Hungarian Intergovernmental Scientific and Technological Cooperation Project (grant no. 2021–07).

Declarations

Ethics approval Not applicable.

Consent to participate Not applicable.

Consent for publication Not applicable.

Conflict of interest The authors declare no competing interests.

References

1. Geier N, Paulo Davim J, Szalay T (2019) Advanced cutting tools and technologies for drilling carbon fibre reinforced polymer (CFRP) composites: a review. Compos Part A 125:105552. https://doi.org/10.1016/j.compositesa.2019.105552
2. Fleischer J, Teti R, Lanza G et al (2018) Composite materials parts manufacturing. CIRP Ann 67:603–626. https://doi.org/10.1016/j.cirp.2018.05.005
3. Xu J, Yin Y, Paulo Davim J et al (2022) A critical review addressing drilling-induced damage of CFRP composites. Compos Struct 294:115594. https://doi.org/10.1016/j.compstruct.2022.115594

4. Panwar NL, Kaushik SC, Kothari S (2011) Role of renewable energy sources in environmental protection: a review. Renew Sust Energy Rev 15:1513–1524. https://doi.org/10.1016/j.rser.2010.11.037
5. Czigány T (2006) Special manufacturing and characteristics of basalt fiber reinforced hybrid polypropylene composites: mechanical properties and acoustic emission study. Compos Sci Technol 66:3210–3220. https://doi.org/10.1016/j.compscitech.2005.07.007
6. Czigány T, Vad J, Pölöskei K (2005) Basalt fiber as a reinforcement of polymer composites. Period Polytech Mech Eng 49:3–14
7. Deák T, Czigány T (2009) Chemical composition and mechanical properties of basalt and glass fibers: a comparison. Text Res J 79:645–651. https://doi.org/10.1177/0040517508095597
8. Amuthakkannan P, Manikandan V, Uthayakumar M (2015) Analysis of delamination in drilling of basalt fiber reinforced polymer composites. Mater Phys Mech 1–8
9. Navarro MD, Meseguer MD, Sánchez A, Gutiérrez S (2017) Tool wear study in edge trimming on basalt fibre reinforced plastics. Procedia Manuf 13:259–266. https://doi.org/10.1016/j.promfg.2017.09.067
10. Navarro-Mas MD, García-Manrique JA, Meseguer MD et al (2018) Delamination study in edge trimming of basalt fiber reinforced plastics (BFRP). Materials. https://doi.org/10.3390/ma11081418
11. Navarro-Mas M, Meseguer M, Lluch-Cerezo J, Garcia-Manrique J (2020) Comparison of different parameters to evaluate delamination in edge trimming of basalt fiber reinforced plastics (BFRP). Materials 13:5326. https://doi.org/10.3390/ma13235326
12. Ahmad J (2009) Machining of polymer composites. Springer, US
13. Li H, Qin X, He G et al (2016) Investigation of chip formation and fracture toughness in orthogonal cutting of UD-CFRP. Int J Adv Manuf Technol 82:1079–1088. https://doi.org/10.1007/s00170-015-7471-x
14. Wang F, Yin J, Ma J et al (2017) Effects of cutting edge radius and fiber cutting angle on the cutting-induced surface damage in machining of unidirectional CFRP composite laminates. Int J Adv Manuf Technol 91:3107–3120. https://doi.org/10.1007/s00170-017-0023-9
15. Hintze W, Clausen R, Schütte C, Kroll K (2018) Evaluation of the total cutting force in drilling of CFRP: a novel experimental method for the analysis of the cutting mechanism. Prod Eng 12:431–440. https://doi.org/10.1007/s11740-018-0807-2
16. Calzada KA, Kapoor SG, DeVor RE et al (2012) Modeling and interpretation of fiber orientation-based failure mechanisms in machining of carbon fiber-reinforced polymer composites. J Manuf Process 14:141–149. https://doi.org/10.1016/j.jmapro.2011.09.005
17. Turki Y, Habak M, Velasco R, Vantomme P (2017) Highlighting cutting mechanisms encountered in carbon/epoxy composite drilling using orthogonal cutting. Int J Adv Manuf Technol 92:685–697. https://doi.org/10.1007/s00170-017-0153-0
18. Geier N, Xu J, Pereszlai C et al (2021) Drilling of carbon fibre reinforced polymer (CFRP) composites: difficulties, challenges and expectations. Procedia Manuf 54:284–289. https://doi.org/10.1016/j.promfg.2021.07.045
19. Poór DI, Geier N, Pereszlai C, Xu J (2021) A critical review of the drilling of CFRP composites: Burr formation, characterisation and challenges. Compos Part B Eng 223:109155. https://doi.org/10.1016/j.compositesb.2021.109155
20. Xu J, Lin T, Li L et al (2022) Numerical study of interface damage formation mechanisms in machining CFRP/Ti6Al4V stacks under different cutting sequence strategies. Compos Struct 285:115236. https://doi.org/10.1016/j.compstruct.2022.115236
21. Hrechuk A, Bushlya V, Ståhl J-E (2018) Hole-quality evaluation in drilling fiber-reinforced composites. Compos Struct 204:378–387. https://doi.org/10.1016/j.compstruct.2018.07.105
22. Xu J, An Q, Chen M (2014) A comparative evaluation of polycrystalline diamond drills in drilling high-strength T800S/250F CFRP. Compos Struct 117:71–82. https://doi.org/10.1016/j.compstruct.2014.06.034
23. Xu J, Li C, Mi S et al (2018) Study of drilling-induced defects for CFRP composites using new criteria. Compos Struct 201:1076–1087. https://doi.org/10.1016/j.compstruct.2018.06.051
24. Geier N, Szalay T, Takács M (2018) Analysis of thrust force and characteristics of uncut fibres at non-conventional oriented drilling of unidirectional carbon fibre-reinforced plastic (UD-CFRP) composite laminates. Int J Adv Manuf Technol 100:3139–3154. https://doi.org/10.1007/s00170-018-2895-8
25. Pereszlai C, Geier N (2020) A comparative analysis of wobble milling, helical milling and conventional drilling of CFRP. Int J Adv Manuf Technol 106:3913–3930. https://doi.org/10.1007/s00170-019-04842-4
26. Pereszlai C, Geier N, Poór DI et al (2021) Drilling fibre reinforced polymer composites (CFRP and GFRP): an analysis of the cutting force of the tilted helical milling process. Compos Struct 262:113646. https://doi.org/10.1016/j.compstruct.2021.113646
27. Geier N, Poór DI, Pereszlai C, Tamás-Bényei P (2022) Drilling of recycled carbon fibre–reinforced polymer (rCFRP) composites: analysis of burrs and microstructure. Int J Adv Manuf Technol. https://doi.org/10.1007/s00170-022-08847-4
28. Geier N, Poór DI, Pereszlai C et al (2022) A drilling case study in polymer composites reinforced by virgin and recycled carbon fibres (CFRP and rCFRP) to analyse thrust force and torque. Int J Adv Manuf Technol. https://doi.org/10.1007/s00170-022-08947-1
29. Xiao J, Gao C, Wang G, Huang P (2019) Investigation on the effects of microstructure on machining unidirectional carbon fiber reinforced polymer composites with a modified force model. J Reinf Plast Compos 0731684419828179. https://doi.org/10.1177/0731684419828179
30. Geier N, Szalay T (2017) Optimisation of process parameters for the orbital and conventional drilling of uni-directional carbon fibre-reinforced polymers (UD-CFRP). Measurement 110:319–334. https://doi.org/10.1016/j.measurement.2017.07.007
31. Fu R, Jia Z, Wang F et al (2018) Drill-exit temperature characteristics in drilling of UD and MD CFRP composites based on infrared thermography. Int J Mach Tools Manuf 135:24–37. https://doi.org/10.1016/j.ijmachtools.2018.08.002
32. Geier N, Pereszlai C (2020) Analysis of characteristics of surface roughness of machined CFRP composites. Period Polytech 64:67–80. https://doi.org/10.3311/PPme.14436
33. Duboust N, Ghadbeigi H, Pinna C et al (2017) An optical method for measuring surface roughness of machined carbon fibre-reinforced plastic composites. J Compos Mater 51:289–302. https://doi.org/10.1177/0021998316644849
34. Horváth R, Drégelyi-Kiss Á (2015) Analysis of surface roughness of aluminum alloys fine turned: united phenomenological models and multi-performance optimization. Measurement 65:181–192. https://doi.org/10.1016/j.measurement.2015.01.013
35. Teicher U, Rosenbaum T, Nestler A, Brosius A (2017) Characterization of the surface roughness of milled carbon fiber reinforced plastic structures. Procedia CIRP 66:199–203. https://doi.org/10.1016/j.procir.2017.03.282
36. Nguyen T-T (2019) Prediction and optimization of machining energy, surface roughness, and production rate in SKD61 milling. Measurement 136:525–544. https://doi.org/10.1016/j.measurement.2019.01.009
37. Vipindas K, Anand KN, Mathew J (2018) Effect of cutting edge radius on micro end milling: force analysis, surface roughness, and chip formation. Int J Adv Manuf Technol 97:711–722. https://doi.org/10.1007/s00170-018-1877-1
38. Balázs BZ, Geier N, Takács M, Davim JP (2021) A review on micro-milling: recent advances and future trends. Int J

Adv Manuf Technol 112:655–684. https://doi.org/10.1007/s00170-020-06445-w
39. Angelone R, Caggiano A, Improta I et al (2018) Temperature measurements for the tool wear and hole quality assessment during drilling of CFRP/CFRP stacks. Procedia CIRP 67:416–421. https://doi.org/10.1016/j.procir.2017.12.235
40. Geng D, Liu Y, Shao Z et al (2019) Delamination formation, evaluation and suppression during drilling of composite laminates: a review. Compos Struct 216:168–186. https://doi.org/10.1016/j.compstruct.2019.02.099
41. Babu J, Paul Alex N, Abraham SP et al (2018) Development of a comprehensive delamination assessment factor and its evaluation with high-speed drilling of composite laminates using a twist drill. Proc Inst Mech Eng Part B J Eng Manuf 232:2109–2121. https://doi.org/10.1177/0954405417690552
42. Qi Z, Zhang K, Li Y et al (2014) Critical thrust force predicting modeling for delamination-free drilling of metal-FRP stacks. Compos Struct 107:604–609. https://doi.org/10.1016/j.compstruct.2013.07.036